IEEE Access
Multidisciplinary ⋮ Rapid Review ⋮ Open Access Journal

Received 29 March 2023, accepted 9 April 2023, date of publication 17 April 2023, date of current version 24 April 2023.

Digital Object Identifier 10.1109/ACCESS.2023.3267851

RESEARCH ARTICLE

Modified Two-Channel LLC Resonant Converter With Optimal Efficiency for Wide Input Voltage Applications

LINLIN PI
School of Automation and Electrical Engineering, Tianjin University of Technology and Education, Tianjin 300355, China
Tianjin Light Industry Vocational Technical College, Tianjin 300354, China
e-mail: pilinlin2022@126.com

ABSTRACT A modified two-channel LLC resonant converter with optimal efficiency for wide input voltage applications. The converter has the same voltage gain and power handing ability as conventional full-bridge (FB) resonant converter, but the hardware cost is lower than conventional FB resonant converter, and the operational frequency range is narrower than conventional resonant converter for the same working condition. It has the characteristics of low input impedance at low input voltage, which is used to provide high voltage gain, and high input impedance at high input voltage, which is used to provide low voltage gain, the above characteristics are analyzed and optimized to improve the efficiency for photovoltaic applications where wide voltage gain is require. A 1 kW prototype is developed, the input voltage ranges from 80 V to 200 V, the output voltage and output power are 400 V and 1 kW, the experimental result shows that the full-load efficiency can reach 96.5% over the entire input voltage range, and the peak efficiency can reach 96.9% at full-load state.

INDEX TERMS Resonant converter, photovoltaic, wide input voltage, high efficiency, DC/DC conversion.

VARIABLES

S_1, S_2	Primary MOSFETs.
D_1, D_2, D_3, D_4	Secondary diodes.
C_{r1}, C_{r2}	Resonant capacitors.
T_1, T_2	Transformers.
L_{m1}, L_{m2}	Magnetizing inductors of T_1 and T_2.
C_o	Output capacitor.
R_o	Equivalent resistor of load.
L_{r1}, L_{r2}	Resonant inductors.
i_{in}	Input current.
i_{S1}, i_{S2}	Currents flowing through S_1 and S_2.
i_{r1}, i_{r2}	Currents flowing through L_{r1} and L_{r2}.
i_{m1}, i_{m2}	Magnetizing currents of T_1 and T_2.
i_{Ts1}, i_{Ts2}	Currents flowing through secondary windings of T_1 and T_2.
i_{Co}	Currents flowing through C_o.
i_{Ro}	Currents flowing through R_o.
N_{T1}, N_{T2}	Turn ratio of T_1 and T_2.
U_{in}	Input voltage.
U_o	Output voltage.
p_1, p_2	Driving signals of S_1 and S_2.
f_s	Switching frequency.
f_{r1}	Resonant frequency.
t_d	Dead time.
T_s	Switching period.
u_{ab}	Voltage between points a and b.
u_{bc}	Voltage between points b and c.
u_{de}	Voltage between points d and e.
u_{fg}	Voltage between points f and g.
$u_{Lm1,FH}$, $u_{Lm2,FH}$	Fundamental voltage across L_{m1} and L_{m2}.
I_o	Average output current.
R_{ac1}, R_{ac2}	Ac equivalent resistors of load resistors.
G_{LLC1}, G_{LLC2}	Voltage gains of two channels.
G_{TCLLC}	Voltage gain of two-channel LLC resonant converter.

The associate editor coordinating the review of this manuscript and approving it for publication was Xiaofeng Yang.

Q	Power quality.
k	Ratio of L_m to L_r.
f_n	Normalized frequency.
G_{HBLLC}	Voltage gain of HB LLC resonant converter.
G_{FBLLC}	Voltage gain of FB LLC resonant converter.
$P_{c,loss}$	Conduction loss.
I_r	RMS resonant current.
I_S	MOSFET current.
I_{Ts}	Transformer secondary windings' current.
$I_{d,avg}$	Diode's average current.
R_{Lr}	ESR of resonant inductor.
R_{Tp}	ESR of primary winding.
R_{Ts}	ESR of secondary winding.
R_{on}	MOSFET's on-resistor.
$V_{F,d}$	Diode's forward voltage-drop.
$P_{s,loss}$	Switching loss.
$I_{S,off}$	Turn-off current of MOSFETs.
t_{fall}	Fall-time of MOSFETs.
$P_{fe,loss}$	Ferrite loss.
V_T	Cores' volume of transformers.
V_{Lr}	Cores' volume of inductors.
K_T, α_T, β_T	Parameters representing property of transformers' cores.
K_{Lr}, α_{Lr}, β_{Lr}	Parameters representing the property of resonant inductors' cores.
ΔB_T, ΔB_{Lr}	Flux density swings of transformers and resonant inductors.
μ_0, μ_e	Space and effective permeabilities.
N_{turn}	Turn number.
I_{max}	Maximum current of windings.
l_e	Effective magnetic loop length.
$P_{ot,loss}$	The other loss's loss.
$P_{dr,loss}$	Driving loss.
$P_{esr,loss}$	PCB ESR's loss.
Q_g	MOSFET's charge.
U_{dr}	Driving voltage.
R_{esr}	System's ESR.
I_{esr}	Current flowing through R_{esr}.
η_{theory}	Theoretical efficiency.
AP_{Lr}	Area product of resonant inductors.
AP_T	Area product of transformers.
Δi_{r1}, Δi_{r2}	Peak-to-peak values of i_{r1} and i_{r2}.
J_{Lr}	Current design of resonant inductors.
$K_{Lr,u}$	Window utility factor of resonant inductors.
B_{Lr}	Flux density of inductor of resonant inductors.
g_{Lr}	Air-gap length of resonant inductors.
l_{Lr}	Length of magnetic loop of resonant inductors.
$\mu_{Lr,r}$, $\mu_{Lr,e}$	Relative and effective permeabilities of resonant inductors.
$I_{p,rms}$	Primary RMS currents of transformers.
$I_{s,rms}$	Secondary RMS currents of transformers.
$f_{s,min}$	Minimum switching frequency.
ΔB_T	Variation of flux density of transformers.
J_T	Current design of transformers.
$K_{T,u}$	Window utility factor of transformers.
N_{Tp}	Primary turn number of transformers.
$I_{m,max}$	Maximum magnetizing current.
$A_{T,e}$	Effective area of magnetic cores.
N_{Ts}	Secondary turn number.
$u_{Cr,max}$	Voltage across resonant capacitor.
$I_{r,pk}$	Peak resonant current.
ω_s	Angular frequency.
t_d	Dead time.
$t_{d,min}$	Minimum dead time.
$t_{d,max}$	Maximum dead time.
$f_{s,max}$	Maximum switching frequency.
C_{oss}	MOSFETs' output capacitance.
θ	Phase angle between the current of the inductor and its voltage.

I. INTRODUCTION

For many applications, such as uninterruptible power supply (UPS) [1], [2], photovoltaic system [3], etc., where electrical isolation and wide voltage gain are needed, because the input voltage varies in wide range and the output voltage is constant, isolated dc/dc converter with wide voltage gain is widely adopted. For photovoltaic applications, the input voltage varies with the irradiation, then the converters should have the ability to operate in wide input voltage. Phase shifted full-bridge (PSFB) [4], [5] and LLC resonant converter [6], [7], [8], [9], [10] are commonly used for wide input voltage applications, because the attractive merits of wide voltage gain and soft-switching. However, the lagging switches make PSFB lose the soft-switching at the light load. On the contrary, LLC resonant converter can soft switch over the entire input voltage range, therefore, it is suitable for photovoltaic application [1], [11].

Traditional parallel-series LLC resonant converters must operate in wide frequency range to realize wide voltage gain conversion, which brings two problems: (a) the operating frequency at the low voltage gain region is extremely high and results in high switching loss, 2) the circulating current at the high voltage gain region is large and results in large conduction loss and massive magnetic volume. LLC resonant converter has two typical configurations, including half bridge (HB) and full bridge (FB) configurations. Considering the electrical limitations of real power switches, HB LLC resonant converter only has the half power handing ability

of FB LLC resonant converter, but FB LLC resonant converter must operate with much high frequency at low voltage region, which results in large switching loss. On the contrary, HB LLC resonant converter can avoid the above problem. Therefore, high efficiency in wide voltage gain range can be solved by combing the merits of HB and FH LLC resonant converters.

The efficiency and electrical stress are also important for wide voltage conversion. Many researches are conducted to decrease the switches' electrical stress. For example, paralleled converters and switches are used to reduce current stress in [12], but the converter's hardware structure is complicated and it is hard to balance the current flowing through the paralleled power switches. In [1], [9], [13], [14], [15], and [16], modified HB LLC resonant converter is adopted to increase the power handling ability with low current stress, and two-channel LLC structure is used to reduce the current stress of the power switches [1], [9], [13], but the operating frequency and switching loss at the low voltage gain is too high.

The scheme in [17] combining HB LLC and FB LLC resonant converters in an interleaved way can also obtain wide gain, but the auxiliary channel makes the hardware configuration complicated. To widen the voltage gain, a reconfigurable LLC resonant converter is proposed in [18], but the converter's control and hardware are more complex. The integrated three-phase HB LLC resonant converter in [19], [20] is also a useful scheme to obtain wide voltage gain, but the current stress of the power switches on the primary side is high, and the conduction loss is high. Some studies are conducted to narrow the operating frequency to reduce the switching loss. For example, an auxiliary switch is used to adjust the impedance in [9], and an optimized control strategy with two split resonant branches in [1] is also proposed to narrow the operating frequency range, but the auxiliary switch in [9] makes the hardware structure complicated, and the control in [1] needs to judge several working states and the realization is difficult. Moreover, the dynamic response needs further improvement because the fluctuation at the mode switching point is large. To simplify the hardware structure, a modified two-channel LLC converter is proposed in [21]. It has only 2 power switches in the primary side but must use full-controlled power switches in the secondary side with phase shift control. The control is more complex than that in [1] and [9] and the requirement and cost of the sampling circuit is higher. For the photovoltaic application, simple configuration [12], high efficiency [22], low cost [23], and high power are required. If LLC resonant converter is applied for photovoltaic, the configuration, efficiency and control need further study to realize high efficiency in wide voltage with simple hardware structure.

In this paper, a modified two-channel LLC resonant converter with high efficiency is proposed for wide input voltage applications. The converter has simple structure on the primary side with only 2 primary power switches, which is the half number of traditional LLC resonant converters in [1], [9], [12], [13], [14], and [15]. Moreover, the converter has two working mode, including HB mode and FB mode. Two modes can provide wide voltage gains with high efficiency through flexible combination. The converter has low impedance and provides high voltage gain when the input voltage is low. Compared with traditional FB and HB LLC converters, the proposed LLC resonant converter can provide wide voltage gain with high efficiency.

II. TWO-CHANNEL LLC RESONANT CONVERTER

A. TOPOLOGY

The topology of two-channel LLC resonant converter is presented in Fig.1. It consists of two complementary parallel-series LLC channels. S_1 and S_2 are primary MOSFETs. D_1-D_4 are secondary diodes. C_{r1} and C_{r2} are resonant capacitors. $C_{r1} = C_{r2} = C_r$. T_1 and T_2 are transformers. L_{m1} and L_{m2} are magnetizing inductors of T_1 and T_2. $L_{m1} = L_{m2} = L_m$. C_o is output capacitor. R_o is the equivalent resistor of load. L_{r1} and L_{r2} are the resonant inductors. To decrease device count number, L_{r1} and L_{r2} can be integrated by a core. i_{in} is the input current. i_{S1} and i_{S2} are the currents flowing through S_1 and S_2. i_{r1} and i_{r2} are the currents flowing through L_{r1} and L_{r2}. i_{m1} and i_{m2} are the magnetizing currents of T_1 and T_2. i_{Ts1} and i_{Ts2} are the currents flowing through the secondary windings of T_1 and T_2. i_{Co} and i_{Ro} are the currents flowing through C_o and R_o, respectively. N_{T1} and N_{T2} are the turn ratio of T_1 and T_2. $N_{T1} = N_{T2} = N_T$. U_{in} and U_o are the input voltage and output voltage. p_1 and p_2 are the driving signals of S_1 and S_2.

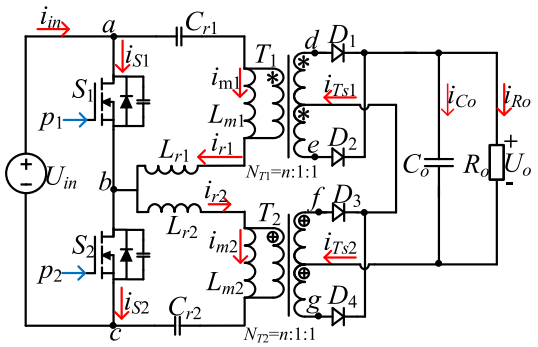

FIGURE 1. Topology of two-channel LLC resonant converter.

B. OPERATIONAL PRINCIPLE

Fig.2(a), (b) and (c) present the waveforms when $f_s < f_{r1}$, $f_s = f_{r1}$ and $f_s > f_{r1}$, respectively. t_d is the dead time. T_s is the switching period. f_s is the switching frequency. $f_{r1} = 0.5\pi^{-1}(L_r C_r)^{-0.5}$ is the resonant frequency. u_{ab} is the voltage between points a and b. u_{bc} is the voltage between points b and c. u_{de} is the voltage between points d and e. u_{fg} is the voltage between points f and g. Two channels are complementary. $i_{r1} = -i_{r2}$. $i_{m1} = -i_{m2}$. u_{ab}, u_{de}, i_{S1}, i_{r1}, i_{m1}

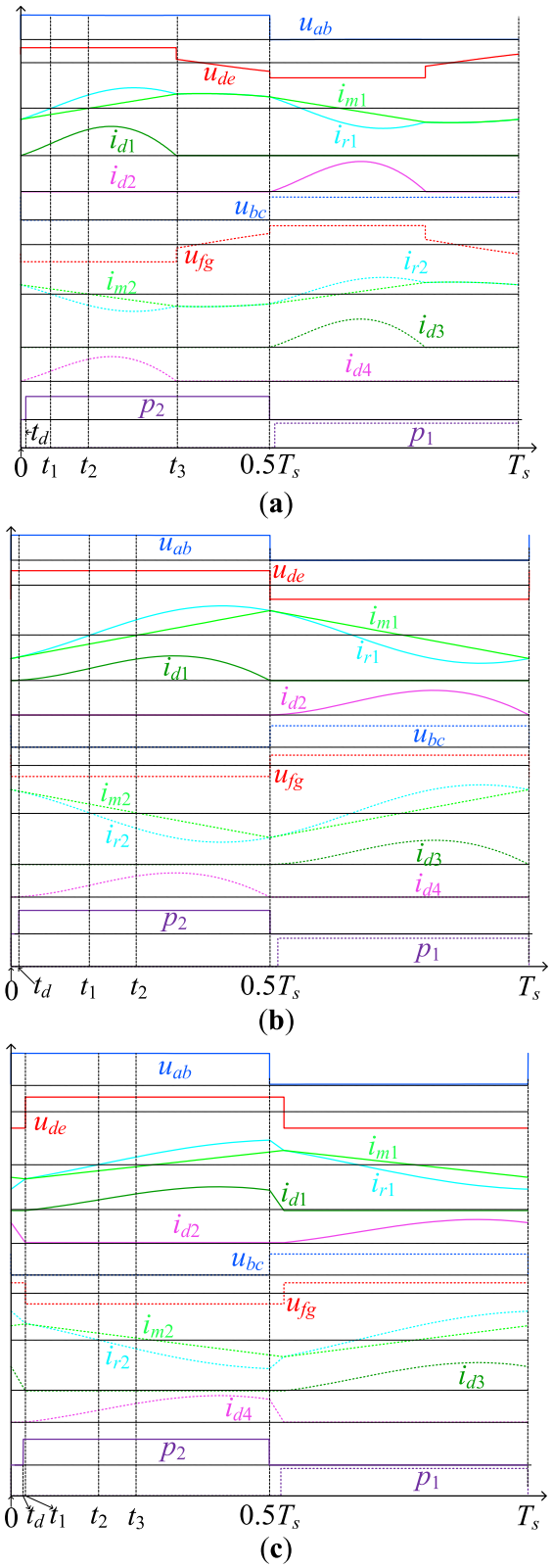

FIGURE 2. Waveforms of two-channel LLC resonant converter when: (a) $f_s < f_{r1}$, (b) $f_s = f_{r1}$, and (c) $f_s > f_{r1}$.

and i_{Ts1} in the former half switching period are symmetry with that in the latter half switching period.

When $f_s < f_{r1}$, the converter works in the capacitive area. A former half switching period can be divided into 5 intervals, including $0 \le t < t_d$, $t_d \le t < t_1$, $t_1 \le t < t_2$, $t_2 \le t < t_3$, and $t_3 \le t < 0.5T_s$. During $0 \le t < t_d$, as Fig3(a) shows, S_1 is turned off, the flowing direction of i_{S2} is negative, D_1 and D_4 are conducting, D_2 and D_3 are blocked, i_{r1} feeds energy from LLC channel back to U_{in}, i_{L1} and i_{L2} discharge the output capacitor of S_2 and make S_2 zero-voltage turn on, where $i_{S2} = i_{r1} + i_{r2}$. During $t_d \le t < t_1$, as Fig.3(b) shows, S_1 is still turned off, S_2 is turned on, the flowing direction of i_{S2} is negative, D_1 and D_4 are conducting, D_2 and D_3 are blocked off. During $t_1 \le t < t_2$, as Fig.3(c) shows, $S_1$is still turned off and S_2 is turning on, the flowing direction of i_{r1} is positive, D_1 and D_4 are conducting, D_2 and D_3 are blocked off. During $t_2 \le t < t_3$, as Fig.3(d) shows, S_1 is still turned off and S_2 is turned on, the flowing direction of i_{S2} is positive, D_1 and D_4 are conducting, D_2 and D_3 are blocked off. During $t_3 \le t < 0.5T_s$, as Fig.3(e) shows, S_1 is still turned off, S_2 is turned on, D_1-D_4 are blocked off, i_{in} transfers energy to resonant tank, C_o provides energy for R_o, the flowing direction of i_{S2} is positive.

When $f_s = f_{r1}$, a former half switching period can be divided into 4 intervals, including $0 \le t < t_d$, $t_d \le t < t_1 t_1 \le t < t_2$, and $t_2 \le t < 0.5T_s$. During $0 \le t < t_1$, the working state of the converter can be illustrated by Fig.3(a). During $t_d \le t < t_1$, the working state of the converter can be illustrated by Fig.3(b). During $t_1 \le t < t_2$, the working state of the converter can be illustrated by Fig.3(c). During $t_2 \le t < 0.5T_s$, the working state of the converter can be illustrated by Fig.3(d).

When $f_s > f_{r1}$, the converter works in the inductive area. A former half switching period can be divided into 5 intervals, including $0 \le t < t_d$, $t_d \le t < t_1$, $t_1 \le t < t_2$, $t_2 \le t < t_3$ and $t_3 \le t < t_4$. During $0 \le t < t_1$, the working state of the converter is as shown in Fig.4, the flowing directions of i_{r1} and i_{m1} are negative, the flowing directions of i_{r2} and i_{m2} are positive, S_1 is turned off and S_2 is turning on, D_1 and D_4 are blocked off, D_2 and D_3 are conducting. During $t_d \le t < t_1$, the working state of the converter can be illustrated by Fig.3(a). During $t_1 \le t < t_2$, the working state of the converter can be illustrated by Fig.3(b). During $t_2 \le t < t_3$, the working state of the converter can be illustrated by Fig.3(c). During $t_3 \le t < 0.5T_s$, the working state of the converter can be illustrated by Fig.3(d).

Two channels can transfer energy from the input side to the output side with complementary phase. The parameters of two channel can be designed as the same. It is useful to simplify the design work. Because each LLC channel only need to take the half power, the volume of resonant components and transformers are much smaller compared with FB and FB LLC resonant converters. Then the hardware cost is lower than traditional FB and HB LLC resonant converters. Moreover, each magnetic component in two-channel LLC resonant converter is smaller, the conductor used in the proposed two-channel LLC resonant converter is less than that of conventional FB LLC resonant converter. Because the

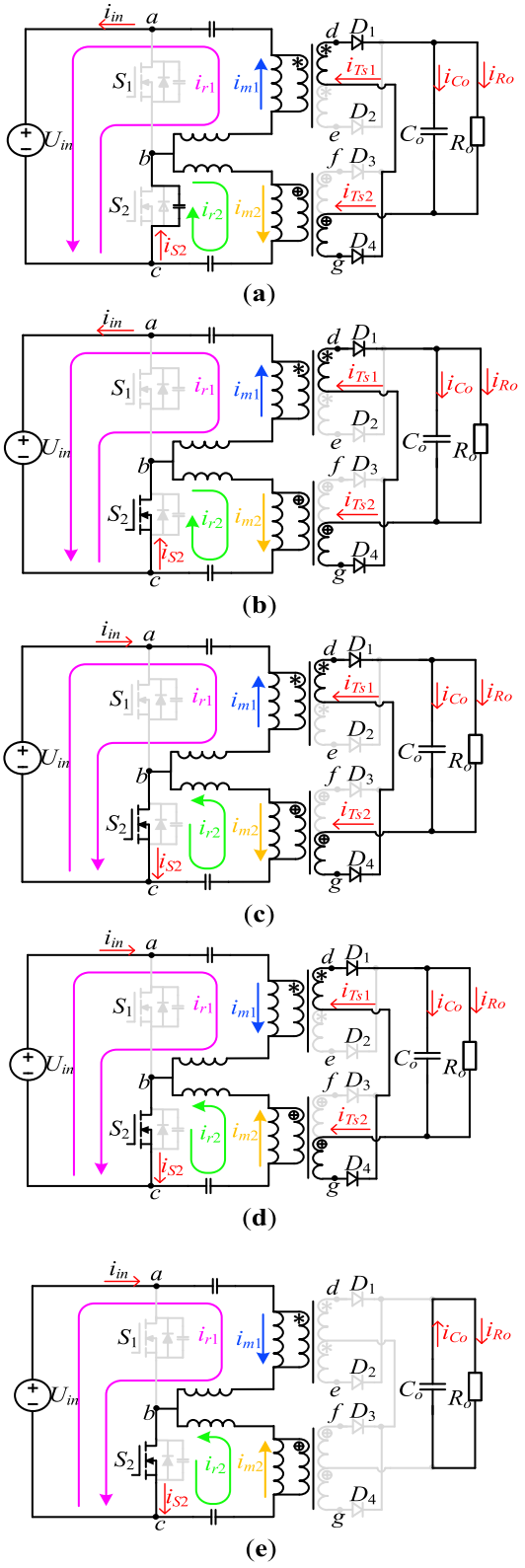

FIGURE 3. States of the converter when: (a) $0 < t \le t_d$, (b) $t_d < t \le t_1$, (c) $t_1 < t \le t_2$, (d) $t_2 < t \le t_3$, and (e) $t_3 < t \le 0.5T$ in the case of $f_s < f_{r1}$.

mean length per turn in the proposed two-channel LLC resonant converter is shorter than that in conventional FB LLC

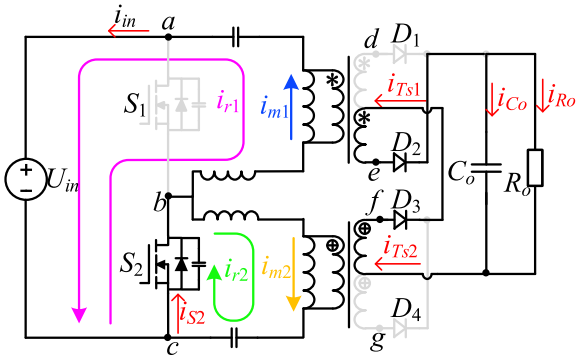

FIGURE 4. State of converter during $0 \le t < t_1$ when $f_s > f_{r1}$.

resonant converter, then the cost of the proposed two-channel LLC resonant converter is less than the cost of conventional FB LLC resonant converter.

C. VOLTAGE GAIN

Fundamental harmonic approximation (FHA) method, time domain method and the combination of the above two methods are commonly used to analyze the voltage gain. Time domain method can accurately analyze the voltage gain, but the process and calculation are complicated. FHA method can relative easily to analyze voltage gain with analytical expressions. In this paper, FHA method is used. Assuming all devices are ideal and two LLC channels have the same parameters, the equivalent circuit can be given in Fig.5. It can be seen as two HB LLC converters with input sources paralleled and output voltage in series.

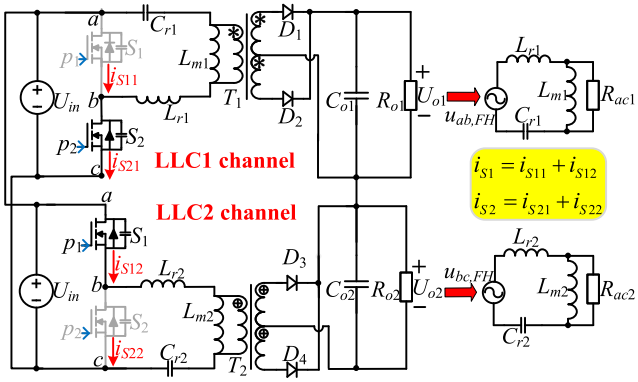

FIGURE 5. Equivalent circuits of the converter.

During S_1 is turned off and S_2 is turned on, the converter works as a HB LLC converter. i_{S1} and i_{S2} are the currents flowing through S_1 and S_2.

$$i_{S1}(t) = i_{S11}(t) + i_{S12}(t) \tag{1}$$

$$i_{S2}(t) = i_{S21}(t) + i_{S22}(t). \tag{2}$$

Two channels' output voltages are the same. Then the voltage across the magnetizing inductors is [21], [22], and [23]

$$u_{Lm1,FH}(t) = \frac{4U_{o1}}{\pi}\sin(2\pi f_s t) = \frac{2U_o}{\pi}\sin(2\pi f_s t) \quad (3)$$

$$u_{Lm2,FH}(t) = \frac{2U_o}{\pi}\sin(2\pi f_s t - \pi). \quad (4)$$

The currents of secondary windings can be expressed as

$$i_{Ts1}(t) = \sqrt{2}\, I_{Ts1,FH}\sin(2\pi f_s t - \theta) \quad (5)$$

$$i_{Ts2}(t) = \sqrt{2}\, I_{Ts2}\sin(2\pi f_s t - \pi - \theta). \quad (6)$$

where $I_{Ts1,FH}$ and $I_{Ts2,FH}$ are the RMS currents of secondary diodes. $I_{Ts1,FH} = I_{Ts2,FH} = I_{rect,FH}$. The average output current I_o is

$$I_o = \frac{2}{T_s}\int_0^{T_s}\left|i_{Ts1,FH}(t)\right|dt = \frac{U_{o1}}{0.5R_o} = \frac{U_o}{R_o} \Rightarrow I_{Ts,FH} = \frac{\pi U_o}{2\sqrt{2}\,R_o}. \quad (7)$$

Then R_{ac1} and R_{ac2} are

$$R_{ac1} = R_{ac2} = \frac{N_T^2 u_{Lm1,FH}(t)}{i_{Ts1,FH}(t)} = \frac{N_T^2 2U_o/\pi}{\sqrt{2}\pi\, U_o \Big/ \left(2\sqrt{2}\,R_o\right)} = \frac{4N_T^2 R_o}{\pi^2} \quad (8)$$

where $R_o = U_o^2/P_o$. P_o is output power. The voltage gains of two channels are

$$G_{LLC1} = G_{LLC2} = \frac{\left|\frac{j\omega_s L_{m1}R_{ac1}}{j\omega_s L_{m1}+R_{ac1}}\right|}{2\left|j\omega_s L_r + \frac{1}{j\omega_s C_r} + \frac{j\omega_s L_{m1}R_{ac1}}{j\omega_s L_{m1}+R_{ac1}}\right|} = \frac{1}{2}\sqrt{\left(1+\frac{1}{k}-\frac{1}{kf_n^2}\right)^2 + Q^2\left(f_n - \frac{1}{f_n}\right)^2} \quad (9)$$

where $Q = (L_r/C_r)^{1/2}/R_{ac1}$ is quality factor. $k = L_m/L_r$. $f_n = f_s/f_r$ is normalized frequency. f_r is the resonant frequency. $\omega_s = 2\pi f_s$ is angular frequency. The voltage gain is

$$G_{TCLLC}(k, Q, f_n) = \frac{U_o}{U_{in}} = G_{LLC1} + G_{LLC2} = 2G_{LLC1} = \sqrt{\left(1+\frac{1}{k}-\frac{1}{kf_n^2}\right)^2 + Q^2\left(f_n - \frac{1}{f_n}\right)^2}. \quad (10)$$

Fig.6 shows the curves of relationships between G_{TCLLC}, G_{FBLLC} and G_{HBLLC} with f_n, where G_{TCLLC}, G_{FBLLC} and G_{HBLLC} are the voltage gains of the studied LLC, FB LLC and HB LLC converters. The voltage gain of the studied converter almost is equal to that of FB LLC converter in the capacitive area. This characteristic can be used to provide high voltage gain. In the capacitive area, the curve of voltage gains by FHA method is closed to that by simulation method. However, in the inductive area, the curve by simulation method is away from the curve by FHA method, because FHA method only concerns the effect of fundamental component but ignores the influence of higher harmonics.

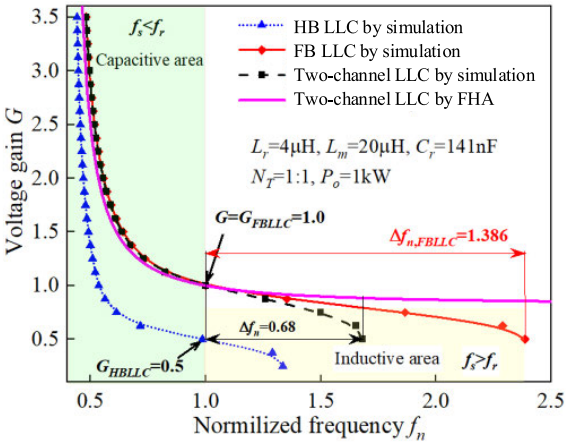

FIGURE 6. Voltage gains of three LLC converters for $L_r = 4\mu$H, $L_m = 20\mu$H, $C_r = 141$nF, $U_i = 200$V, $N_T = 1{:}1$ and $P_o = 1$kW.

As Fig.6 shows, for FB LLC converter, if the required voltage gain ranges from 0.5 to 1.0, the normalized frequency $f_{n,FBLLC}$ ranges from 1.0 to 2.386. The frequency's variation $\Delta f_{n,FBLLC}$ is about 1.386. However, for the studied converter, $f_{n,TCLLC}$ just ranges from 1.0 to 1.68. The $\Delta f_{n,TCLLC}$ is only 0.68, which is 0.706 less than $\Delta f_{n,FBLLC}$.

D. EFFICIENCY

The power loss of the converter includes conduction loss, switching loss, ferrite loss and the other loss. The other loss is mainly caused by the driving circuit and the equivalent series resistors (ESRs) of the printed circuit board (PCB), surface mounted technology (SMT) components, etc. The conduction loss $P_{c,loss}$ is [24]

$$P_{c,loss} = 2\left[\begin{array}{l} I_r^2(R_{Lr}+R_{Tp}) + I_S^2 R_{on} \\ +I_{Ts}^2 R_{Ts} + V_{F,d} I_{d,avg} \end{array}\right] \quad (11)$$

where I_r, I_S, and I_{Ts} are RMS resonant current, MOSFET current, and transformer secondary windings' current, respectively. $I_{d,avg}$ is diode's average current. R_{Lr}, R_{Tp}, T_{Ts} are the ESRs of resonant inductor, primary and the secondary windings, respectively. R_{on} is the on-resistor of MOSFETs. $V_{F,d}$ is the forward voltage-drop of diodes.

The switching loss $P_{s,loss}$ is [24]

$$P_{s,loss} = 2\times 0.5 I_{S,off}\, U_{in} t_{fall} f_s = I_{S,off}\, U_{in} t_{fall} f \quad (12)$$

where $I_{S,off}$ and t_{fall} are the turn-off current and fall-time of MOSFETs, respectively. $I_{S,off} = i_{r1}(0.5T_s)$. The ferrite loss $P_{fe,loss}$ is [3]

$$P_{fe,loss} = 2\left(V_T K_T \Delta B_T^{\alpha_T} f_s^{\beta_T} + V_{Lr} K_{Lr} \Delta B_{Lr}^{\alpha_T} f_s^{\beta_T}\right) \quad (13)$$

where V_T and V_{Lr} are the cores' volume of transformers and inductors, respectively. K_T, α_T and β_T are parameters representing the property of transformers' cores. K_{Lr}, α_{Lr}

and β_{Lr} are parameters representing the property of resonant inductors' cores. ΔB_T and ΔB_{Lr} are the flux density swings of transformers and resonant inductors. $\Delta B = 2\mu_0\mu_e N_{turn} I_{max}/l_e$. μ_0 and μ_e are the space and effective permeabilities, respectively. N_{turn} is turn number. I_{max} is the maximum current of windings. l_e is the effective magnetic loop length.

The other loss $P_{ot,loss}$ mainly consists of the driving loss and the PCB ESR's loss. $P_{oth,loss}$ is estimated by [24]

$$P_{ot,loss} = P_{dr,loss} + P_{esr,loss} = 2Q_g U_{dr} f_s + I_{esr}^2 R_{esr} \quad (14)$$

where $P_{dr,loss}$ and $P_{esr,loss}$ are the driving loss and the PCB ESR's loss. Q_g is the MOSFET's charge. U_{dr} is the driving voltage. R_{esr} is the system's ESR. I_{esr} is the current flowing through R_{esr}. The theoretical efficiency η_{theory} is

$$\eta_{c,TCLLC} = \frac{P_o}{P_o + P_{c,loss} + P_{s,loss} + P_{fe,loss} + P_{ot,loss}}. \quad (15)$$

Fig.7 shows the curve of relationship between the theoretical efficiency and the input voltage, where $P_o = 1$kW, $U_o = 400$ V. U_{in} ranges from 80 V to 200 V.

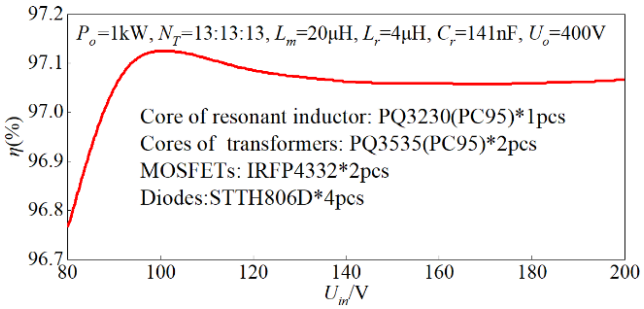

FIGURE 7. Curve of relationship between efficiency and voltage.

The cores for the inductors and transformers are PQ3230(PC95) and PQ3535(PC95), respectively. S_1-S_2 and D_1-D_4 are IRFP4332 MOSFETs and STTH806D diodes. AWG#38 × 350 wire is adopted for the inductors. AWG#38 × 350 and AWG#38 × 70 wires are used for the primary and the secondary windings of the transformers. The air-gap lengths of the inductors and transformers are 2.65mm and 1mm, respectively. The turn number of the inductors is 10. The turn ratio of the transformers is 13:13:13. When the input voltage ranges from 80V to 200V, the theoretical efficiency is higher than 96.7%. At $U_{in} = 100$V, the converter reaches the peak efficiency. The peak efficiency is about 97.1%.

E. CONTROL

U_o is a constant value. U_{in} varies a lot. f_s also varies with U_{in}. A closed control scheme is needed to adjust f_s according to the voltage's variation. Fig.8 presents the control scheme. PI controller is adopted for the voltage loop. $U_{o,ref}$ is the reference output voltage. Delay unit is used to set dead time. k_p is the proportional coefficient. k_i is the integrator coefficient. p_1 and p_2 are the triggering signals of S_1 and S_2, respectively.

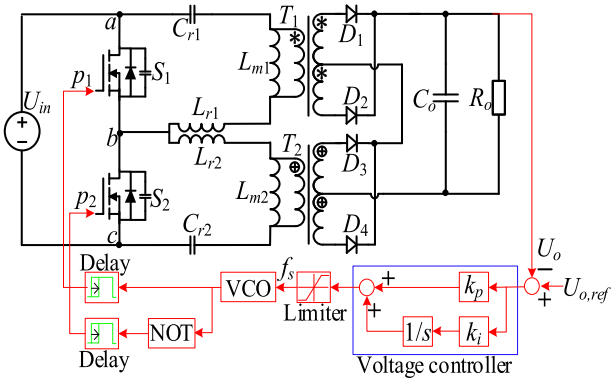

FIGURE 8. Control scheme of two-channel LLC resonant converter.

F. COMPARISONS

Fig.9 shows the RMS current of transformer. Both the RMS currents flowing through the primary and secondary windings are lower than that of traditional FB LLC and HB LLC converters.

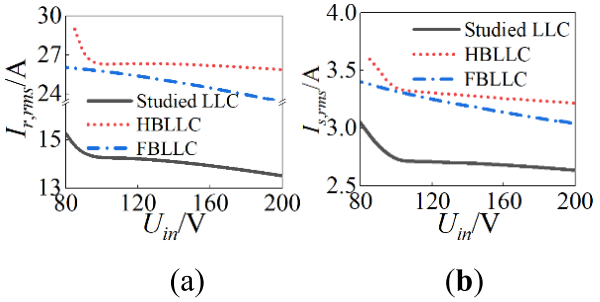

FIGURE 9. RMS current of transformers': (a) primary, and (b) secondary windings.

Table.1 shows the voltage stress for three kinds of converters. The diodes' voltage stress for the converter is the half of traditional converter.

TABLE 1. Voltage stress.

Voltage stress	This paper	HB LLC	FB LLC
MOSFET	U_{in}	U_{in}	U_{in}
Diode	U_o	$2U_o$	$2U_o$

III. CONSIDERATIONS OF DESIGN

A. RESONANT INDUCTOR

The area product AP_{Lr} is used to design inductor. AP_{Lr} is [1]

$$AP_{Lr} = \frac{4L_r I_r \Delta i_r}{J_{Lr} K_{Lr,u} \Delta B_{Lr}} \quad (16)$$

where $I_{r1} = I_{r2} = I_r$. Δi_{r1} and Δi_{r2} are the peak-to-peak values of i_{r1} and i_{r2}. $\Delta i_{r1} = \Delta i_{r2} = \Delta i_r$. J_{Lr}, $K_{Lr,u}$ and B_{Lr} are the current density, window utility factor and flux density

of inductor. The turn number N_{Lr} is

$$N_{Lr} = \frac{4L_r i_{r,max}}{A_{Lr,e}\Delta B_{Lr}} \tag{17}$$

where $i_{r1,max}$ and $i_{r2,max}$ are the maximum current of L_{r1} and L_{r2}. $i_{r1,max} = i_{r2,max} = i_{r,max}$. $A_{Lr,e}$ is the effective area of core. The length g_{Lr} of air-gap is

$$g_{Lr} = 0.5 l_{Lr}\left(\frac{1}{\mu_{Lr,e}} - \frac{1}{\mu_{Lr,r}}\right) \tag{18}$$

$$\mu_{Lr,e} = \frac{L_r l_{Lr}}{\mu_0 N_{Lr}^2 A_{Lr,e}} \tag{19}$$

where l_{Lr} is the length of magnetic loop. $\mu_{Lr,r}$ and $\mu_{Lr,e}$ are the relative and effective permeabilities, respectively.

B. TRANSFORMERS

The area product AP_T is calculated by [5]

$$AP_T = \frac{2U_o\left(I_r N_T + I_{s,rms}\right)}{f_{s,min}\Delta B_T J_T K_{T,u}} \tag{20}$$

where $I_{p,rms}$ and $I_{s,rms}$ and the primary and secondary RMS currents of transformers, respectively. $f_{s,min}$ is the minimum switching frequency. ΔB_T, J_T and $K_{T,u}$ are the flux density, current density and window utility factor of transformers.

As Fig.6 shows, the voltage gain can be accurately analyzed by FHA method in the capacitive area. However, in the inductive area, FHA method will lead large error. To simplify the analyses of voltage gain, the converter is designed to work in the capacitive area. On this occasion, the minimum voltage gain point can be seen as the normal working point. The turn ratio of transformers can be designed at this point.

$$N_T = \frac{U_{in,max}}{U_{o1}} = \frac{U_{in,max}}{0.5U_o}. \tag{21}$$

$$N_{Tp} = \frac{2L_m I_{m,max}}{\Delta B_T A_{T,e}} \tag{22}$$

where N_{Tp} is the primary turn number. $I_{m,max}$ is the maximum magnetizing current. $A_{T,e}$ is the effective area of magnetic cores. The secondary turn number $N_{Ts} = N_{Tp}/N_T$.

C. RESONANT CAPACITORS

The voltage across resonant capacitor is

$$u_{Cr,max} = I_{r,pk}X_{Cr} = \frac{I_{r,pk}}{\omega_s C_r} \tag{23}$$

where $I_{r,pk}$ is peak resonant current. $\omega_s = 2\pi f_s$ is angular frequency.

D. DEAD TIME

The ZVS condition of MOSFETs is ensured by the design of dead time t_d. Generally, t_d is much smaller than T_s. During t_r, i_{r1} and i_{r2} fully discharge MOSFETs' output capacitors and make the voltage decrease from U_i to 0 V, while the RMS currents and conduction loss are influenced by t_d. With above consideration, t_d should be in the range of [5] and [6]

$$t_{d,min} \le t_d \le t_{d,max} \tag{24}$$

$$t_{d,min} = 16 f_{s,max} C_{oss} \tag{25}$$

$$t_{d,max} = \frac{I_{Ts}^2 R_{ac}^2}{U_o^2 f_{r1}} - \frac{0.5}{f_{r1}} - \frac{\sqrt{12\left(1-\pi^2\right)U_o^4 + 768 I_{Ts}^4 R_{ac}^4 + \frac{N_T^4 R_{ac}^2 U_o^4 (48-5\pi^2)}{\pi^2 L_m^2 f_{r1}^2}}}{12 U_o^2 f_{r1}} \tag{26}$$

where $f_{s,max}$ is the maximum switching frequency. C_{oss} is MOSFETs' output capacitance. $t_{d,min}$ and $t_{d,max}$ are the lower and upper limitations of t_d.

E. DESIGN FLOW

The design flow is given in Fig.10. Firstly, $U_{in,min}$, $U_{in,max}$, U_o, P_o, $f_{s,max}$, $f_{s,min}$ and η are obtained based on requirements. Then N_T is determined by (21). k and the initial values of L_m. L_r and C_r are set. R_{ac} and Q are accordingly figured out. The voltage gain is obtained by FHA method.

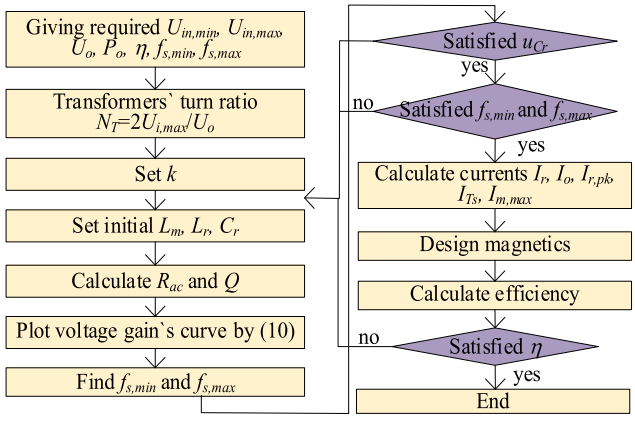

FIGURE 10. Control scheme of the converter.

If the requirements are not satisfied, the flow jumps back the 4th step to adjust L_m, L_r and C_r. Otherwise, the flow continues. After magnetics are designed, the theoretical efficiency can be estimated. If the requirement is also satisfied, the design flow is ended.

IV. SIMULATION AND EXPERIMENTAL RESULTS

Table 2 shows the requirements. The $f_{s,min}$ and $f_{s,max}$ are 80kHz and 200kHz, respectively. The minimum voltage gain G_{min} and the maximum voltage gain G_{max} are 2 and 5, respectively. Combining the requirements in Table 2 and the design flow in Fig.8, a set of parameters are obtained and presented in Table 3.

Fig.11 shows the dynamic simulation results of two-channel LLC resonant converter when U_{in} gradually decreases from 200V to 80V. It can be seen that the variation of U_o is smaller than 3V and the dynamic regulating ability

for U_o of the converter is well. Moreover, the resonant currents of two LLC channels are also stable in the dynamic process.

TABLE 2. Voltage stress.

Symbol	Quantity
U_{in}	80 V-200 V
U_o	400 V
P_o	1 kW
f_s	80 kHz-120 kHz
η	96 %
G_{min}	2
G_{max}	5

TABLE 3. Voltage stress.

Symbol	Quantity
L_r	4 μH
C_r	141 nF
L_m	20 μH
N_{Lr}	2×10
N_T	13:13

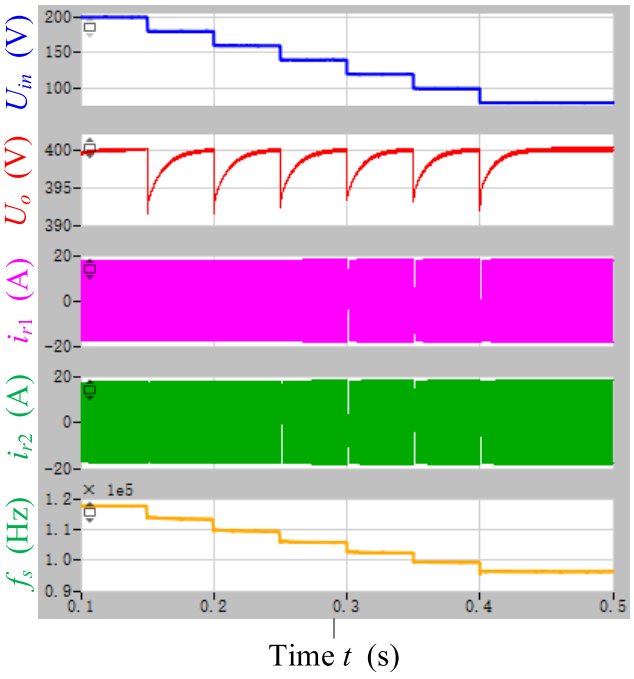

FIGURE 11. Dynamic simulation waveforms of two-channel LLC resonant converter.

Based on the design result, a 1 kW prototype is developed, Fig.12 shows the picture. The measured u_{ab}, u_{de}, u_{fg}, p_1, i_{r1}, i_{r2}, i_{Ts1}, i_{Ts2} are given in Fig.12. i_{r1} and i_{r2} are complementary. i_{Ts1} and i_{Ts2} almost are the same.

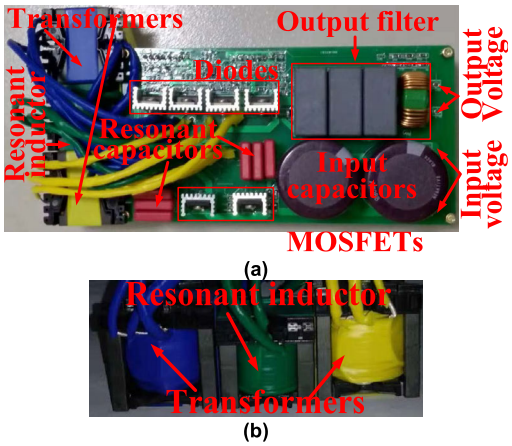

FIGURE 12. Pictures of: (a) prototype and (b) magnetics.

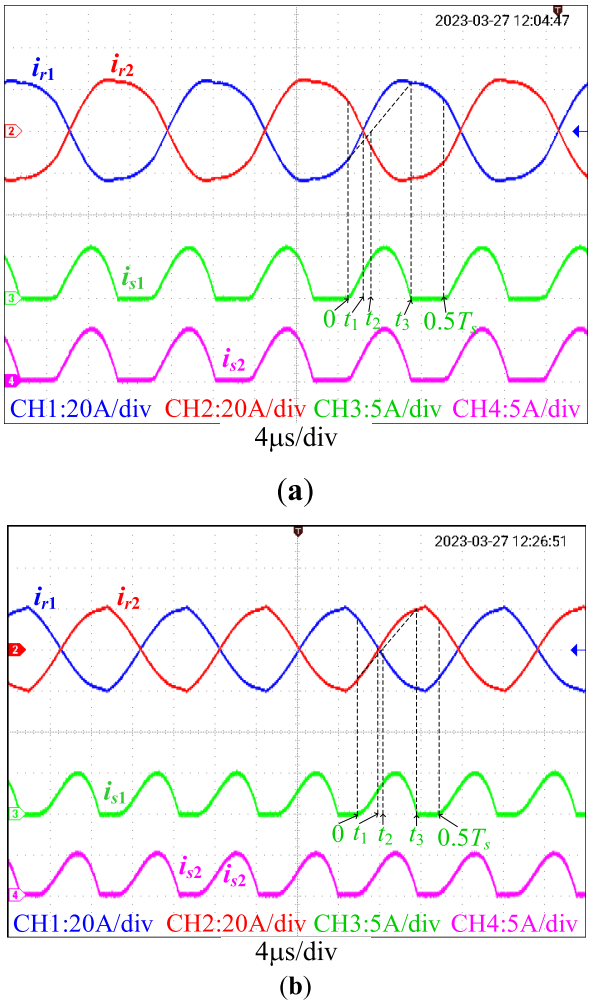

FIGURE 13. Measured: (a) i_{r1}, i_{r2}, i_{s1}, i_{s2} at U_{in} = 80V and full load state, and (b) i_{r1}, i_{r2}, i_{s1}, i_{s2} at U_{in} = 200V and full load state.

Fig.13(a) presents the measured i_{r1}, i_{r2}, i_{s1}, and i_{s2} when U_{in} = 80V at the full-load state. Fig.13(b) shows the

measured i_{r1}, i_{r2}, i_{s1}, and i_{s2} when $U_{in} = 200$V at the full-load state. Compared with Fig.12(a), the peak resonant current in Fig.13(a) is greater.

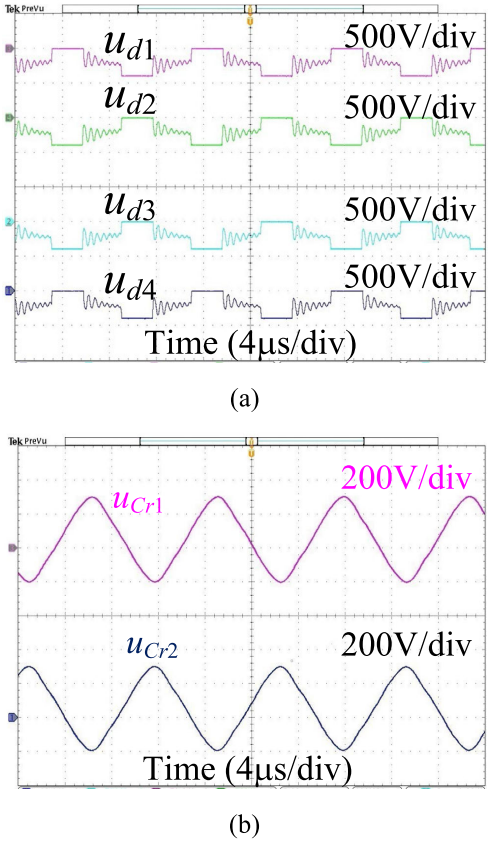

FIGURE 14. Measured: (a) diodes' voltage, and (b) resonant capacitor's voltage for U_{in} = 80V, U_o = 400V and P_o = 1kW.

Fig.14(a) presents the measured voltage across diodes u_{d1}, u_{d2}, u_{d3} and u_{d4}. The voltage stress of diodes is 400V, which is equal to U_o. The peak value of u_{Cr} appears at U_{in} is minimum. Because $U_{in,min}$ = 80V, the maximum u_{Cr} is measured at U_{in} = 80V and presented in Fig.14(b). The theoretical maximum u_{Cr} is about 317V. Fig.14(b) shows that the measured maximum of u_{Cr} is about 293V. The error is about 8%. The reason for this is that FHA method ignores the effect of higher harmonics.

Fig.15(a), 15(b), and 15(c) show the loss distribution at U_{in} = 80V, 140V and 200V, respectively. Over the entire input voltage range, the MOSFETs' loss accounts for about 60% of total loss, this is attributed to the large RMS MOSFET's current. The RMS MOSFET's current decreases with the increase of U_{in}. Then the conduction loss reduces with the increase of U_{in}. The MOSFETs' switching loss is relative smaller than the conduction loss. The diodes' loss is almost a constant because that P_o and the average secondary current are almost constant. The ferrite loss is more than the copper loss. The magnetizing current and the maximum magnetic flux density increase with the increase of U_{in}. Moreover, f_s also increases with the increase of U_{in}. Then the ferrite loss increases with the increase of U_{in}. The inductors' loss decreases with the increase of U_{in}. The inductor's ferrite loss is relative smaller than the inductor's copper loss. The copper loss is mainly determined by the winding's ac ESR and the RMS current flowing through windings. Because the copper loss has square relationship with the RMS current. Additionally, the decease of the RMS current flowing through resonant inductor's windings with the increase of input voltage is faster than the increase of the winding's ac ESR with the increase of U_{in}. Then the copper loss decreases with the increase of U_{in}.

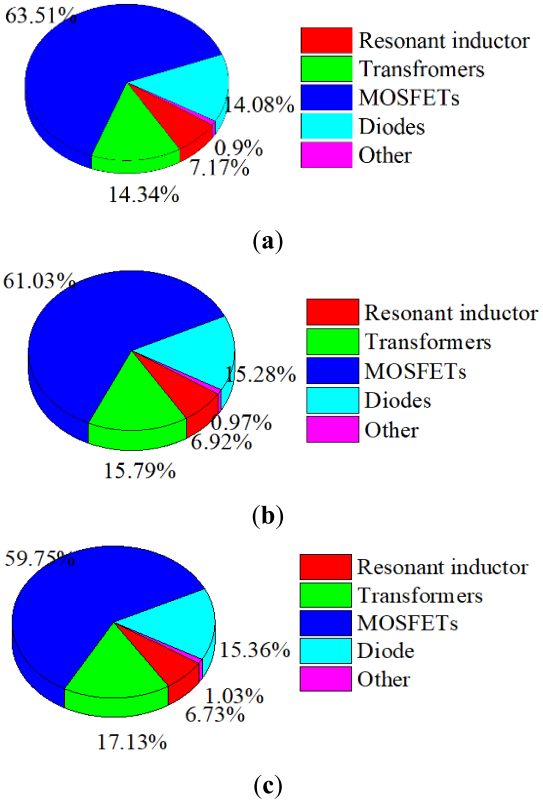

FIGURE 15. Loss distribution at U_{in} =: (a)80V, (b)140V, and (c)200V.

The other loss mainly consists of the driving loss. Because the driving loss is determined by switching frequency and the switching frequency increases with the increase of U_{in}, the driving loss increases with the increase of U_{in}.

Fig.16 shows the measured curves of relationship between f_s and U_o. When U_{in} ranges from 80V to 200V, f_s varies between 87.4kHz and 107.45kHz. The converter's frequency variation Δf_s is 20.05kHz.

Fig.17 presents the measured efficiency over the entire input voltage range. The full-load efficiency of two-channel LLC resonant converter is higher than 96.5%. The peak efficiency is about 96.9% when IRFP4332 MOSFET and STTH806D diode are adopted. If the above adopted MOSFET is replaced by IPZ60R017C7, the efficiency of

TABLE 4. Comparisons.

Items	Two-channel LLC	HB LLC [1]	FB LLC [1]
Output power	1kW	1kW	1kW
Input voltage	80V-200V	80V-200V	80V-200V
Output voltage	400V	400V	400V
Peak efficiency	96.9%	97.5%	96.78%
Resonant inductor	1×PQ3230, L_r=4μH	2×PQ3220, L_r=4.6μH	1×RM14, L_r=10.5μH
Transformers	2×PQ3535, L_m=20μH	1×PQ4040+1×PQ3535, L_m=17μH	2×PQ4040, L_m=28μH
Resonant capacitance	141nF	141nF	120nF
Magnetics` volume	46.6 ml	61.8 ml	54.9 ml
Normalized voltage gain	2-5	2-5	2-5
Magnetics` power density	21.5 kW/l	16.2 kW/l	18.2 kW/l
Primary devices	2×IRFP4332	4×IRFP4332	4×IRFP4332
Secondary devices	4×STTH806D	4×STTH806D	4×STTH806D
Driving channel`s number	2	4	4
Cost per kilowatt	low	high	high
Control	pulse frequency modulation	pulse frequency modulation	pulse frequency modulation
Single component volume	small	large	small
Power density	high	low	low
Current stress of power switches	low	high	low

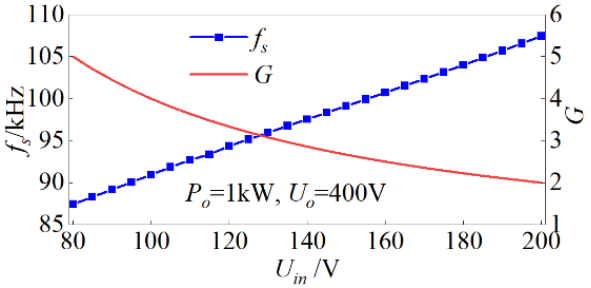

FIGURE 16. Measured curves of relationship between f_s and U_{in}.

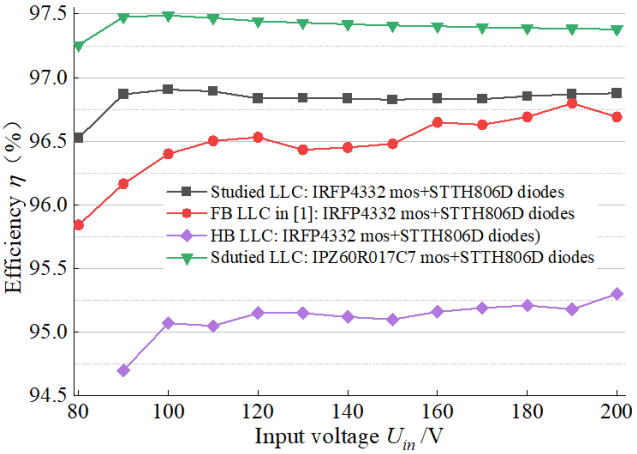

FIGURE 17. Measured curves of relationship between η and U_{in}.

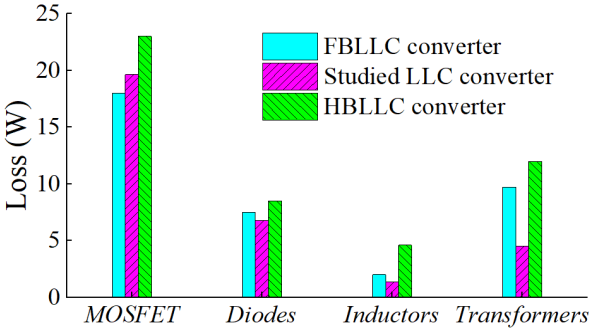

FIGURE 18. Losses for three LLC converters at full load state.

two-channel LLC resonant converter can increase to 97.2%. the peak efficiency can increase to 97.5%. Because the on-resistor of IPZ60R017C7 MOSFET is much smaller than the on-resistor of IRFP4332 MOSFET, the conduction loss in the case that IPZ60R017C7 MOSFET is adopted is much lower than the conduction loss in the case that IRFP4332 MOSFET is adopted.

Table 4 presents the comparison for three LLC converters. The magnetics' power density of the converter is 21.5 kW/L, which is 3.3 kW/l and 8.3kW/l higher than that of conventional FB and HB LLC converters in [1]. Moreover, the prototype has a higher peak efficiency and lower cost compared with traditional LLC converters. Fig.18 shows the calculated loss when $U_o = 400$V, $U_{in} = 200$V and $P_o = 1$kW. The prototype's loss is lower than that of conventional LLC converters.

Fig.19 shows the measured output voltage u_o and the resonant current i_r during the start-up process. The whole start-up time is about 1.1ms and has no impulse during the start-up process.

Fig.20 shows the measured output voltage u_o and the resonant current i_r when the load factor from 20% to 100%. The output voltage can keep stable during the load varies. Fig.19 and Fig.20 verify that the converter can stably works during the working states changes.

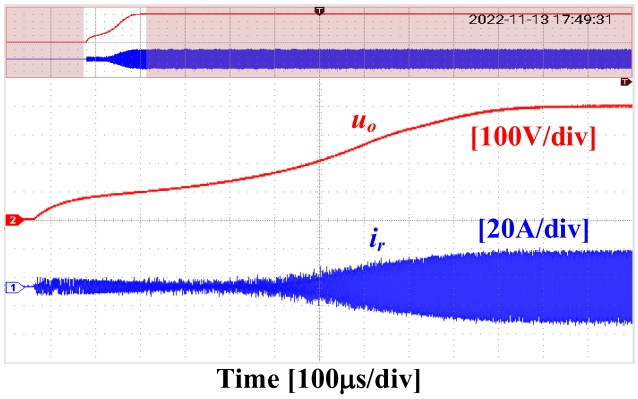

FIGURE 19. Measured output voltage and resonant current during the start-up process.

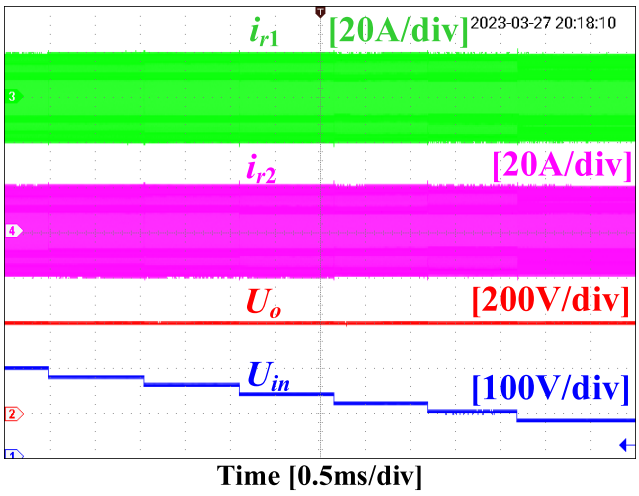

FIGURE 20. Measured output voltage and resonant current when the load factor increases from 20% to 100%.

V. CONCLUSION

A parallel-series resonant LLC converter with high efficiency and wide voltage gain is studied for photovoltaic applications. A 1 kW prototype is developed. The efficiency is higher than 97.2% over the entire input voltage. The peak efficiency is 97.5% appearing at $U_{in} = 100$V. The converter has the following advantages:

(a) There are only 2 power switches in the primary side. Only two driving channels are required, which is useful to reduce the hardware cost of photovoltaic system. The power handling ability is the same as traditional FB LLC converter, which is useful to increase the power density of photovoltaic system.

(b) The converter has high input impedance at high input voltage, which is helpful to provide low voltage gain with higher efficiency during the photovoltaic array's voltage is relatively high.

(c) The converter has low input impedance at low input voltage, which is useful to provide high voltage gain with high efficiency when the photovoltaic array's output voltage is relatively low.

Moreover, the studied converter can be also used for the applications where wide voltage, narrow frequency, high efficiency, and high power are required, such as, on-board charger, battery storage system, etc.

APPENDIX A

The RMS values of i_r, i_{Ts} and the peak resonant current $I_{r,pk}$ can be calculated by [7]

$$I_r = \sqrt{\frac{N_T^2 U_o^2 f_s}{32 L_m^2 f_{r1}^2}\left(\frac{2}{f_s} - \frac{1}{f_{r1}}\right) + \frac{\pi^2 I_o^2 f_{r1}^2}{8 N_T^2 f_s^2}} \tag{a1}$$

$$I_{Lm,max} = \frac{N_T U_o}{4 L_m f_{r1}} \tag{a2}$$

$$i_{Ts}(t) = \begin{cases} N_T I_{r,pk} \sin(\omega_r t + \varphi) \\ \quad + \frac{N_T^2 U_o}{4 L_m f_{r1}} & \text{if } 0 \le t < \frac{1}{2f_r} \\ \quad - \frac{N_T^2 U_o}{L_m} t \\ 0 & \text{if } \frac{1}{2f_r} \le t < \frac{1}{2f_s} \end{cases} \tag{a3}$$

$$\varphi = \tan^{-1}\left(-\frac{N_T^2 R_o f_s}{2\omega_r L_m f_r}\right) \tag{a4}$$

$$I_{Ts} = \sqrt{f_s \int_0^{T_s} i_{Ts}^2(t) dt} \tag{a5}$$

$$I_{r,pk} = \sqrt{\left(\frac{\pi I_o f_{r1}}{2 N_T f_s}\right)^2 + I_{Lm,\max}^2}. \tag{a6}$$

REFERENCES

[1] W. Sun, Y. Xing, H. Wu, and J. Ding, "Modified high-efficiency LLC converters with two split resonant branches for wide input-voltage range applications," *IEEE Trans. Power Electron.*, vol. 33, no. 9, pp. 7867–7879, Sep. 2018.

[2] C. Wang, S. Chu, Y. Ying, A. Wang, R. Chen, H. Xu, and B. Zhu, "Underfrequency load shedding scheme for islanded microgrids considering objective and subjective weight of loads," *IEEE Trans. Smart Grid*, vol. 14, no. 2, pp. 899–913, Mar. 2023.

[3] S. M. S. I. Shakib and S. Mekhilef, "A frequency adaptive phase shift modulation control based LLC series resonant converter for wide input voltage applications," *IEEE Trans. Power Electron.*, vol. 32, no. 11, pp. 8360–8370, Nov. 2017.

[4] L. Zhao, H. Li, X. Wu, and J. Zhang, "An improved phase-shifted full-bridge converter with wide-range ZVS and reduced filter requirement," *IEEE Trans. Ind. Electron.*, vol. 65, no. 3, pp. 2167–2176, Mar. 2018.

[5] L. Yi, Q. Gui, and Z. Wang, "A novel phase-shifted pulse width amplitude modulation for extended-boost quasi-Z source cascaded multilevel inverter based on photovoltaic power system," *J. Renew. Sustain. Energy*, vol. 11, no. 1, Jan. 2019, Art. no. 015304.

[6] U. Kundu and P. Sensarma, "A unified approach for automatic resonant frequency tracking in LLC DC–DC converter," *IEEE Trans. Ind. Electron.*, vol. 64, no. 12, pp. 9311–9321, Dec. 2017.

[7] C. Liu, H. Liu, G. Cai, S. Cui, H. Liu, and H. Yao, "Novel hybrid LLC resonant and DAB linear DC–DC converter: Average model and experimental verification," *IEEE Trans. Ind. Electron.*, vol. 64, no. 9, pp. 6970–6978, Sep. 2017.

[8] S.-W. Kang and B.-H. Cho, "Digitally implemented charge control for LLC resonant converters," *IEEE Trans. Ind. Electron.*, vol. 64, no. 8, pp. 6159–6168, Aug. 2017.

[9] J. Zhang, J. Liu, J. Yang, N. Zhao, Y. Wang, and T. Q. Zheng, "An LLC-LC type bidirectional control strategy for an LLC resonant converter in power electronic traction transformer," *IEEE Trans. Ind. Electron.*, vol. 65, no. 11, pp. 8595–8604, Nov. 2018.

[10] X. Sun, X. Li, Y. Shen, B. Wang, and X. Guo, "Dual-bridge LLC resonant converter with fixed-frequency PWM control for wide input applications," *IEEE Trans. Power Electron.*, vol. 32, no. 1, pp. 69–80, Jan. 2017.
[11] O. Kirshenboim and M. M. Peretz, "Combined multilevel and two-phase interleaved LLC converter with enhanced power processing characteristics and natural current sharing," *IEEE Trans. Power Electron.*, vol. 33, no. 7, pp. 5613–5620, Jul. 2018.
[12] H. Hu, X. Fang, F. Chen, Z. J. Shen, and I. Batarseh, "A modified high-efficiency LLC converter with two transformers for wide input-voltage range applications," *IEEE Trans. Power Electron.*, vol. 28, no. 4, pp. 1946–1960, Apr. 2013.
[13] J.-I. Baek, C.-E. Kim, K.-W. Kim, M.-S. Lee, and G.-W. Moon, "Dual half-bridge LLC resonant converter with hybrid-secondary-rectifier (HSR) for wide-ouput-voltage applications," in *Proc. Int. Power Electron. Conf. (IPEC-Niigata ECCE Asia)*, May 2018, pp. 108–113.
[14] Z. Fang, J. Wang, S. Duan, K. Liu, and T. Cai, "Control of an LLC resonant converter using load feedback linearization," *IEEE Trans. Power Electron.*, vol. 33, no. 1, pp. 887–898, Jan. 2018.
[15] M. I. Shahzad, S. Iqbal, and S. Taib, "Interleaved LLC converter with cascaded voltage-doubler rectifiers for deeply depleted PEV battery charging," *IEEE Trans. Transport. Electrific.*, vol. 4, no. 1, pp. 89–98, Mar. 2018.
[16] C. Zhang, Z. Gao, and X. Liao, "Bidirectional DC–DC converter with series-connected resonant tanks to realise soft switching," *IET Power Electron.*, vol. 11, no. 12, pp. 2029–2043, Oct. 2018.
[17] M. Wang, X. Zha, S. Pan, J. Gong, and W. Lin, "A current-sharing method for interleaved high-frequency LLC converter with partial energy phase shift regulation," *IEEE J. Emerg. Sel. Topics Power Electron.*, vol. 10, no. 1, pp. 760–772, Feb. 2022.
[18] G. Li, D. Yang, B. Zhou, and H. Zhang, "A topology-reconfigurable LLC resonant converter for wide output range applications," *IEEE Trans. Veh. Technol.*, vol. 71, no. 10, pp. 10389–10399, Oct. 2022.
[19] G. Li, D. Yang, B. Zhou, Y.-F. Liu, and H. Zhang, "Integration of three-phase LLC resonant converter and full-bridge converter for hybrid modulated multioutput topology," *IEEE J. Emerg. Sel. Topics Power Electron.*, vol. 10, no. 5, pp. 5844–5856, Oct. 2022.
[20] W. Tang, H. Wang, X. Zhu, W. Mo, W. Gao, and X. Yue, "The analysis of current sharing effect for two-unit paralleled common capacitor LLC resonant converter," *IEEE Trans. Ind. Electron.*, vol. 70, no. 3, pp. 2178–2188, Mar. 2023.
[21] D. Zeng, Y. Zhang, T. Li, M. Qi, E. Qi, and G. Zhu, "Reliability research of DC charging module," in *Proc. 43rd Annu. Conf. IEEE Ind. Electron. Soc.*, Oct. 2017, pp. 7958–7962.
[22] Y. Wang, N. Qi, Y. Guan, C. Cecati, and D. Xu, "A single-stage LED driver based on SEPIC and LLC circuits," *IEEE Trans. Ind. Electron.*, vol. 64, no. 7, pp. 5766–5776, Jul. 2017.
[23] S. M. Tayebi and I. Batarseh, "Analysis and optimization of variable-frequency soft-switching peak current mode control techniques for microinverters," *IEEE Trans. Power Electron.*, vol. 33, no. 2, pp. 1644–1653, Feb. 2018.
[24] H. Xu, D. Chen, F. Xue, and X. Li, "Optimal design method of interleaved boost PFC for improving efficiency from switching frequency, boost inductor, and output voltage," *IEEE Trans. Power Electron.*, vol. 34, no. 7, pp. 6088–6107, Jul. 2019.

LINLIN PI received the B.E. degree in computer science and technology from Tianjin Chengjian University and the M.S. degree in information and communication engineering from Tiangong University, China, in 2010. She is currently pursuing the Ph.D. degree with the Tianjin University of Technology and Education. She is also an Associate Professor with the Tianjin Light Industry Vocational Technical College, China. She is the author/coauthor of three books and more than 20 publications in technical journals and conferences. Her research interests include renewable energy and modeling and planning of distribution networks.